26

1 Direct Measurements of Copper Speciation in Basaltic Glasses: Understanding the Relative 2 Roles of Sulfur and Oxygen in Copper Complexation in Melts Antonio Lanzirotti^{a*}, Lopaka Lee^b, Elisabet Head^c, Stephen R. Sutton^a, Matthew Newville^a, 3 Molly McCanta^d, Allan Lerner^e and Paul J. Wallace^e 4 5 ^a Center for Advanced Radiation Sources, The University of Chicago, Chicago 60637, USA 6 ^bHawaiian Volcano Observatory, US Geological Survey, Hawai'i National Park, HI 96718, USA. 7 ^eDepartment of Earth Science, Northeastern Illinois University, Chicago, IL 60625, USA. 8 ^dDepartment of Earth and Planetary Sciences, University of Tennessee, Knoxville, TN 37996, USA. 9 ^e Department of Earth Sciences, University of Oregon, Eugene, OR 97403, USA 10 11 Corresponding author: Dr. Antonio Lanzirotti, Center for Advanced Radiation Sources, The University of Chicago, 12 Chicago, IL 60637, USA. Email: lanzirotti@uchicago.edu. 13 14 **Abstract** 15 Micro-analytical determination of copper (Cu) speciation in natural magmatic glasses, equilibrated below 16 the nickel – nickel oxide (NNO) buffer, reveals that two copper species are commonly stabilized in such 17 basaltic melts. X-ray absorption fine structure (XAFS) spectroscopic analysis of basaltic matrix glasses 18 and melt inclusions (MI) from samples of mid-ocean ridge basalt (MORB), and from Nyamuragira, Etna 19 and Kīlauea volcanoes shows that Cu complexes as both Cu(I)-sulfide and Cu(I)-oxide species in silicate 20 melts. The proportion of each species correlates with the measured sulfur (S) abundance of the glass. In 21 glasses with S abundances greater than ~1000 ppm, Cu(I)-sulfide species are dominant, whereas in 22 glasses with S abundances between 500 and 1000 ppm, both species are found to coexist. The Cu(I)-oxide 23 species dominate at S concentrations below 500 ppm. In 1 atm S-free experimental glasses of basaltic 24 composition that we analyzed, only Cu(I)-oxide species are detectable, regardless of the oxygen fugacity 25 (fO₂), even at relatively high fO₂ values well above the NNO buffer. Our results demonstrate that XAFS

techniques are highly sensitive in measuring Cu speciation in reduced (below NNO) basaltic glasses and

that both oxide and sulfide complexes can be stabilized. The relative proportion of these two species is highly dependent on the concentration of S in the melt, and thus the Cu speciation in natural melts changes as S is lost from the melt by low pressure degassing.

30

31

32

33

34

35

36

37

38

39

40

41

42

43

44

45

46

47

48

49

50

51

27

28

29

1. Introduction

The solubility of metals in silicate melts can be strongly influenced by intrinsic properties of the magma such as pressure, temperature, and melt composition. Understanding how such parameters control metal solubility is important for understanding magma evolution, potential driving mechanisms for core formation in terrestrial planets (Gaetani and Grove, 1997; Holzheid and Lodders, 2001), the conditions that lead to the formation of economically important metallogenic ore deposits (Sillitoe, 1997; Sillitoe, 2010), and the links between volcanic degassing and metal emissions to the atmosphere (Edmonds et al., 2018). For all such phenomena, the partitioning of metals between the melt and metal-bearing minerals, fluids or vapors is of paramount importance, and partitioning is likely to be dependent on the speciation of the metals in the melt phase (Ripley and Brophy, 1995; Gaetani and Grove, 1997; Li and Audétat, 2012; Zajacz et al., 2012; Kiseeva and Wood, 2013). Understanding the controls on copper (Cu) speciation in silicate melts is particularly important for modeling Cu partitioning during mantle melting and for understanding mechanisms for Cu mineralization in ore deposits. Copper is considered a strongly chalcophile element and although it is generally believed that Cu mineralization in terrestrial magmas is related to the availability of reduced sulfur (S²-) in the melt (Lee et al., 2012; Sun et al., 2013; Zhang et al., 2017), it remains unclear how the speciation of dissolved Cu changes with changing sulfur abundance and speciation. For example, porphyry Cu deposits are typically found associated with high fO₂ magmas where sulfur is generally speciated as sulfate (Jugo, 2009; Sillitoe, 2010; Sun et al., 2013). Yet the chalcophilic nature of Cu in these systems generally requires either sulfate reduction or introduction of external sulfide to precipitate Cu mineralization. Similarly, there is still some controversy as to whether residual sulfide must be present or absent during

52 mantle melting to explain the Cu concentrations measured in mantle-derived, mafic magmas (Ripley and 53 Brophy, 1995; Fellows and Canil, 2012; Lee et al., 2012; Kiseeva and Wood, 2013). A better 54 understanding of the speciation of dissolved Cu in melts with changing S concentration and speciation 55

would provide valuable insights to help address these questions.

56

57

58

59

60

61

62

63

64

65

66

67

68

69

70

71

72

73

74

75

76

77

Constraints on Cu speciation in sulfide-saturated silicate melts come largely from experimentallydetermined partition coefficients (Ripley and Brophy, 1995; Gaetani and Grove, 1997; Holzheid and Lodders, 2001; Ripley et al., 2002). Measured partition coefficients will largely be reflective of how Cu is speciated in the melt at the defined conditions. But generally, the speciation of Cu in these experiments is inferred. Although it is not uncommon for formulated equilibrium constant expressions to express the Cu complexation in silicate melts in terms of oxide components (i.e. CuO_{0.5} for Cu¹⁺), this cannot be used to infer that Cu is necessarily stabilized in basaltic melts as an oxide species (Candela and Holland, 1984; Jugo et al., 1999; Ripley et al., 2002). Copper oxide (Holzheid and Lodders, 2001; Ripley et al., 2002; Zajacz et al., 2012; Vigneresse et al., 2014), hydroxide, oxy-sulfide (Ripley et al., 2002), sulfide (Imai et al., 1993; Sillitoe, 1997; Jugo, 2009; Vigneresse et al., 2014), and chloride (Vigneresse et al., 2014) species have all been suggested to be potentially stable in terrestrial silicate melts under certain conditions. Experiments generally show that the oxygen fugacity (fO_2) of the melt can exert a strong control on the measured Cu solubility and partitioning (Gaetani and Grove, 1997; Holzheid and Lodders, 2001; Ripley et al., 2002; Li and Audétat, 2012; Zajacz et al., 2012, 2013). However, many of these same studies have also observed a correlation between measured Cu solubility and the availability of other potential ligands in the melt, in particular S and Cl. Observed correlations with melt S²- concentration have been hypothesized to potentially indicate that, in addition to oxide complexing, some degree of Cu-S complexing may also occur at high melt S contents, possibly stabilizing some Cu in the melt as an oxysulfide species (Ripley et al., 2002; Zajacz et al., 2012). The researchers in these studies have hypothesized that preferential bonding of Cu in the melt to S²- anions relative to O²- would be expected to result in weaker dependency of Cu partitioning with magmatic fO₂ (Peach and Mathez, 1993; Gaetani and Grove, 1997; Ripley et al., 2002).

A direct measurement of Cu speciation in magmatic glasses would provide insight into the compositional parameters controlling Cu solubility in natural systems, particularly in relation to measured natural S abundances. This is important when one considers that Cu abundances in natural silicate melts are typically lower than what are utilized in experimental studies. For example, Cu concentrations in midocean ridge basalts (MORB) average ~ 100 ppm (Prinz, 1967; Sun et al., 2003; Lee et al., 2012), with S concentrations often exceeding 1000 ppm (Wallace and Carmichael, 1992).

Currently, X-ray absorption fine structure (XAFS) spectroscopy is the only available methodology for directly measuring Cu speciation in magmatic glasses at natural concentrations (10-100s ppm). XAFS also provides the only technique available for analyzing metal speciation in melt inclusions (MI), small samples of melt with typical diameters < 100 µm, that are entrapped within growing crystals. Melt inclusion analysis is important for characterizing natural samples with varying S content, as the MI can trap samples of melt within the phenocryst host at depth before the melt has potentially undergone high degrees of degassing (Danyushevsky et al., 2002; Métrich and Wallace, 2008). Analysis of the XAFS can provide information regarding the oxidation state of Cu and the molecular environment around the Cu ion, including coordination geometry and bond disorder. Thus XAFS analysis of natural magmatic glasses should provide a quantitative fingerprint of the molecular species present in the melt (i.e. Kelley and Cottrell, 2009; Head et al., 2011a; Brounce et al., 2015; Moussallam et al., 2016).

This study presents direct measurement of Cu speciation by XAFS in magmatic glasses that have equilibrated below the nickel – nickel oxide (NNO) redox buffer. Results are presented from several volcanic systems, but we primarily focus on samples collected from the 2008-2018 summit eruptions at Halema'uma'u and along the East Rift Zone of Kīlauea Volcano, Hawai'i (Thornber et al., 2015). This suite of samples provides a unique opportunity to systematically evaluate how changes in Cu speciation potentially correlate with magmatic S content in natural melts, given the large observed changes in S concentrations in olivine-hosted MI from this system over 10 years of near continuous eruption, while major element chemistry has remained relatively constant (Thornber et al., 2015; Neal et al., 2018).

2. Methods

103

104

105

106

107

108

109

110

111

112

113

114

115

116

117

118

119

120

121

122

123

124

125

126

127

2.1 Samples and Preparation

Natural samples analyzed include magmatic and volcanic glasses collected at the Kīlauea summit vent, Halema'uma'u, and from the East Rift Zone (ERZ) between 2008 and 2018 (Poland et al., 2008; Thornber et al., 2015). Samples were provided by the United States Geological Survey (USGS) Hawaiian Volcano Observatory (HVO) and primarily consist of hand-picked grain mounts extracted from specimens of tephra and lava that have been single-side polished for analysis. A list of the Kīlauea samples analyzed is presented in Table 1, along with their eruption (and sampling) date. The Kīlauea tephra samples tend to be ~ 2 vol\% olivine-phyric basalts with phenocrysts that regularly contain glassy MI. A set of Kīlauea 2018 samples analyzed are from highly vesicular golden pumice erupted during early high fountaining periods at "fissure 8" of the May – August, 2018 lower ERZ fissure eruption (Neal et al., 2018). All the MI studied here are enclosed within olivine phenocrysts, and many grains preserve attached matrix glass at the phenocryst margins, which was also analyzed when available. Some additional Kīlauea samples were also prepared as doubly polished grain mounts that completely intersect the MI on both surfaces to reduce potential contributions to the analysis from phenocryst and matrix glass material that may underlie the inclusion. Also analyzed were Smithsonian basaltic glass standards VG-2 (NMNH 111240-52, Juan de Fuca Ridge) and A-99 (NMNH 113498-1, collected from Kīlauea summit in 1965). These were both prepared as singly-polished, epoxy-mounted sections. A sample of matrix glass in lapilli erupted from Mt. Etna, Sicily in 2015 was provided for analysis from the Instituto Nazionale di Geofisica e Vulcanologia (Pisa, Italy) collection as a standard thin section. Analysis of olivine-hosted MI (alkaline basalt) from Nyamuragira volcano in D.R. Congo is also presented, prepared as a singly-polished grain mount (see Head et al., 2011; Head et al., 2018 for sample details). Additionally, a sample of pillow-rim basaltic glass dredged from the East Pacific Rise (sample location between ~ 9°46'N and 9°57'N, Fornari et al. 2012) was analyzed. This was prepared as a 30 µm polished thin section on nominally Cu-free quartz

glass, sectioned perpendicular to the glassy outer margin of the pillow (Marescotti et al., 2000). This sample is described in detail in Lanzirotti et al. (2018).

Cu K-edge XAFS spectra were also collected from experimental glasses equilibrated under varying fO_2 conditions for comparison to spectra collected in natural samples. These cover a redox range relative to the NNO buffer from NNO-4.2 to NNO+4.7 and were synthesized from natural basaltic starting materials at 1 atm pressure. Sulfur and chlorine contents were not controlled in these experiments, so we assume that these volatile elements were largely degassed during synthesis. This includes glasses from the Smithsonian NMNH 117393 standard suite (Cottrell et al., 2009), which were synthesized from powdered MORB as a starting material, and from a suite of glasses summarized in Dufresne et al. (2009), which were synthesized from a sample of olivine tholeite from a 1921 flow from Kīlauea (Holloway and Burnham, 1972) as the starting material.

A suite of Cu-bearing crystalline compounds was also analyzed to provide reference spectra for comparison to XAFS measured in the natural samples. These compounds were prepared as powdered samples on tape and were measured in a transmission-mode geometry.

2.2 Analytical Methods

Microscale XAFS analyses were performed at the GSECARS X-ray microprobe beamline (13-ID-E) at the Advanced Photon Source (APS), Argonne National Laboratory (Argonne, IL USA). The GSECARS 13-ID-E beamline utilizes a 3.6 cm period undulator X-ray source that provides X radiation from 2.3 to 28 keV. Monochromatic radiation is provided by a cryogenically-cooled double-crystal monochromator that sits upstream of two horizontally deflecting mirrors with variable mirror coatings that focus the monochromatic beam to a secondary source aperture (SSA). The monochromator has fixed offset and utilizes a state-of-the-art, air-bearing turntable for highly stable rotations throughout the range of selectable energies. The system incorporates both Si(111) and Si(311) crystals, which are translated into the beam as needed. The Si(111) crystal set was used for these experiments. Incident flux was kept to ~ 1.0e¹¹ photons/second for these experiments. Beam focusing to the sample is provided by a set of 240

mm long, highly polished, silicon mirrors (Rh-coated) in a Kirkpatrick-Baez (KB) geometry. Focused spot size for this instrument is $\sim 2~\mu m$ in the horizontal by $\sim 1~\mu m$ in the vertical (FWHM), but for most of the XAFS analyses presented here the beam was purposely defocused to $\sim 10~\mu m$ to reduce flux density on the sample. Measured spectra were normalized to incident intensity (I₀) measured in a helium-filled, 200 mm-long ion chamber just upstream of the KB mirror optics.

All μ-XAFS spectra in glasses were collected in fluorescence mode using a four-element, silicon-drift-diode detector array (Vortex-ME4, Hitachi High-Technologies Science America, Inc.) with pulse-processing provided by an Xspress 3 digital X-ray processor system (Quantum Detectors). All the fluorescence-mode XAFS data collected were corrected for detector dead time. For all samples, a minimum of three spatially distinct XAFS analyses were collected to evaluate reproducibility. In virtually all cases, repeat spectra were indistinguishable to better than 5% reproducibility in edge-step normalized intensity throughout the entire energy range measured. Cu K-edge XAFS was also collected for Cubearing crystalline model compounds to serve as reference, standard spectra, measured in transmission mode using ion chambers.

XAFS spectra were collected with the monochromator scanning energy continuously, with measured intensities binned over given energy intervals. The incident energy was scanned from 8929-8969 eV using 2 eV energy bins, 8969-9009 eV in 0.1 eV bins, and from 9009-9160 eV in 1 eV bins at a scan rate of 3 seconds per energy bin. A zero valent Cu metal foil standard provided an absorption edge energy of 8980.48 eV, in agreement with refined absorption edge energies measured by (Kraft et al., 1996).

Measuring high-quality Cu K-edge XAFS in basaltic glasses using an energy dispersive spectrometer (EDS) proves challenging due to the relatively low Cu abundance (\sim 100 ppm) compared to the much higher concentration of other elements that can overlap with the Cu K α emission. The EDS used here provides a fluorescence energy resolution of \sim 150 eV. The most notable overlap is from Fe, which is present at concentrations of \sim 10 wt% and typically dominates the measured fluorescence signal. We were able to improve detection of the Cu K α emission line through addition of 100 μ m of aluminum to act as a

low energy filter between the sample and detector. The aluminum filtering preferentially lowers the intensity of the Fe emission lines compared to the higher energy Cu fluorescence. Coupled with optimization of the detector solid angle, this allowed us to increase the net counts for Cu K α by a factor of 3.5. Repeat measurements of Cu spectra were used to evaluate potential changes in Cu speciation with time that may indicate beam induced changes in speciation with irradiation. For these particular samples no clear evidence for beam induced changes in Cu valence are observed, although it is worth pointing out we have observed changes in Fe, S and V valence in the natural samples when high flux densities are used during analysis (> 2.5 x 10^{10} photons/s/ μ m²).

The diameter and thickness of the analyzed MI varies between ~ 25 and 300 μm . Analytical points within MI were chosen following microfocused X-ray fluorescence (μ -XRF) compositional mapping of the inclusion in an effort to minimize any potential spectral contribution from the surrounding host mineral, from any potential micro-inclusions that were not visible optically, and to target the thickest parts of MI for analysis. The estimated 1/e attenuation length for Cu K α X-rays in basaltic glass is ~ 60 μm , so some host olivine might be within the analytical excitation volume. However, analysis of the phenocryst hosts shows that Cu concentrations in the surrounding olivine are significantly lower than that measured in the glass, so that the contribution to the measured XAFS spectra is negligible. We also note that XAFS spectra collected on samples with doubly intersected MI are consistent with those measured from contemporaneous samples prepared as singly-polished grain mounts, further indicating insignificant Cu K α signal contributions from any accidentally analyzed olivine hosts in single-sided polished MI.

The Larch XAFS analysis software package (Newville, 2013) was used for spectral processing and for linear combination fitting (LCF) of the Cu XAFS to quantify the relative proportion of Cu species in the glasses analyzed (Table 1). This two-component fitting was done in the normalized $\mu(E)$ space over an energy range of 8970 to 9015 eV using edge-normalized Cu K-edge spectra measured in CuS standard and experimental 1 atm Kīlauea tholeiitic basalt (NNO+4.7) as the predictor components. These were chosen on the basis of their similarity to end-member spectra measured in the natural glasses. The Larch

LCF provides the proportions of each Cu species in the fit, the uncertainties in these proportions, and a calculated *R-factor* (Ravel and Newville, 2005). The calculated *R-factors* (Table 1) are a measure of residuals (*R*) between the fitted and measured spectra, with better fits indicated by lower *R-factors*.

203

204

205

206 Estimated S and Cu abundances (Table 1) were calculated based on measured X-ray fluorescence 207 intensities for the natural glasses. Intensities were measured using synchrotron µ–XRF analysis at 13-ID-208 E and elemental abundances calculated using linear regression calibration of external standards, generally 209 following the methodology described in Sutton et al. (2002) and Lanzirotti et al. (2010). Calibration 210 curves for these abundance estimates are based on analyses of various standard glasses, described below. 211 All were prepared as singly-polished, epoxy mounted samples with thicknesses greater than two 1/e 212 absorption lengths at the Cu K-edge energy. For S, the calibration is based on linear regression of 213 measured S Kα emission intensities, using background subtracted Gaussian peakfit of energy dispersive 214 spectra (triplicate analysis, 60 sec real time, deadtime corrected) measured using a 4 keV incident beam 215 energy with sample and detector in a helium environment. Lower limit of detection (LLD) for S under 216 these filtering conditions is calculated to be ~ 30 ppm. Calibration standards were Smithsonian glass 217 standards NMNH 111240-52 and NMNH 113498-1, using the S abundances reported by LeVoyer on the Smithsonian Mineral Collection data sheet for these standards. The approach for the Cu calibration is 218 219 similar, but using the energy filtering conditions described above for XAFS spectra and an incident beam 220 energy 9.5 keV. LLD for Cu under these filtering conditions is calculated to be ~ 5 ppm, however the 221 LLD is quite sensitive to elevated backgrounds in samples with high amounts of Ni due to spectral 222 overlaps in the energy dispersive spectra. Calibration standards were Smithsonian standard NMNH 223 111240-52 (using abundance reported in Jenner and O'Neill, 2012) and USGS standard glasses GSC-1G, 224 GSD-1G, GSE-1G, and BCR-2G (using abundances reported in Jochum et al., 2005). For estimating Cu 225 abundance in the MI, a thickness correction is required, given that the 1/e attenuation length for Cu Ka 226 X-rays is assumed to be $\sim 60 \mu m$ (based on calculated attenuation for Cu K-radiation in basaltic glass), 227 while MI thicknesses were 25-300 μm. A correction was thus applied based on an estimated inclusion

thickness for each MI (based on optical measurements and XRF mapping) and predicted Cu K α fluorescence yield in basaltic glass, calculated using the NRLXRF program (Criss et al., 1978), following the general methodologies described in Lanzirotti et al. (2008). However, given that the majority of the grain mounts analyzed have only one side of the crystal wafer polished, making an accurate thickness measurement can be difficult. For calculating S abundances in MI, the 1/e attenuation length for S K α X-rays is assumed to be \sim 5 µm (based on calculated attenuation for S K-radiation in basaltic glass) so it was assumed that no thickness correction was required given that all MI were estimated to be thicker than 10 µm. Calculated S concentrations for Kīlauea glasses are consistent with those reported by Thornber et al. (2015) and measurement uncertainties (random error) are estimated to be \sim 13% (1 σ) taking into account regression uncertainties, stated abundance uncertainties for the standards, reproducibility of replicate analyses (for both standards and unknowns), and uncertainties in fitting emission intensities in measured EDS spectra (summation in quadrature). Measurement uncertainties for Cu abundance calculations over the standardized concentration range are estimated to be \sim 15% (1 σ), with uncertainties calculated in a similar manner as with S, but also including reasonable uncertainties in estimated inclusion thickness, which will impact calculated abundances given analysis depths at 9.5 keV.

3. Results

3.1 Copper XAFS Measured in Model Compounds

Figure 1a displays Cu K-edge XAFS spectra collected for Cu-bearing crystalline compounds and aqueous solutions, which we hypothesize to be potentially similar to the chemical species found in silicate melts. The absorption edge energy of the XAFS spectra (generally defined as the energy of half-intensity on the initial rising edge of a spectrum) is diagnostic of Cu valence (Kau et al., 1987). Spectra for Cu¹⁺ species display a rising edge position that is at least 2 eV lower in energy than what is seen for Cu²⁺ species. Spectra for crystalline Cu(I)-oxide (Cu₂O; cuprite) show a sharp, low-energy pre-edge peak which typically displays an intensity approximately half that of the main absorption peak. Spectra for crystalline Cu(I)-sulfides, although broadly similar, show distinct differences in the near-edge that relate

to the coordination of Cu (Pattrick et al., 1997). Chalcocite (Cu₂S) displays a smooth absorption edge between 8982-8983 eV that is assigned to the Cu 1s → 4p electronic transition (Kau et al., 1987), with the broad absorption edge believed to largely reflect the distorted triangular coordination of Cu in the lattice (Pattrick et al., 1997). Chalcopyrite (CuFeS₂), by contrast, displays a small pre-edge peak structure and sharper edge that is indicative of tetrahedrally coordinated Cu. The XAFS spectrum for CuS (covellite) is intermediate to these two spectra, characterized by a rising absorption edge and distinct shoulder that is slightly higher in energy than is found in Cu₂S, but lacking the pre-edge peak structure and sharper absorption edge observed in chalcopyrite (Pattrick et al., 1997). Although it may seem intuitive to assign a formal 2- oxidation state to S and 2+ to Cu in covellite, based on the stoichiometry, studies have shown that CuS lacks Cu²⁺ (d9) ions and is better described as a pyrite-type structure where Cu¹⁺ and S¹⁻ undergo pairing (Goh et al., 2006; Vegelius et al., 2012). It has been suggested the Cu K-edge XAFS observed in covellite is consistent with having a significant proportion of Cu in disordered, trigonal coordination (Pattrick et al., 1997). Crystalline Cu(II) species display spectra that are distinctive from that observed in Cu(I)-oxide and –sulfide species, with edge positions at much higher energy and a maximum in their absorption edge spectra near 8997 eV. Aqueous Cu species that are also potentially relevant for comparison have been analyzed using XAFS

Aqueous Cu species that are also potentially relevant for comparison have been analyzed using XAFS by several researchers (Fulton et al., 2000a; Fulton et al., 2000b; Brugger et al., 2007; Etschmann et al., 2010), generally as aqueous Cu solutions analyzed within pressure cells. Species analyzed include linear Cu(I) complexes (Fulton et al., 2000a; Fulton et al., 2000b) and Cu(II) complexes in a distorted octahedral symmetry. The linear Cu(I) complexes include, for example, linear dichloro Cu¹⁺ species such as $[CuCl_2]^-$ (Fulton et al., 2000a), linear Cu-Cl species such as CuCl(aq) (Fulton et al., 2000a; Brugger et al., 2007) and linear S-Cu-S or O-Cu-S species such as $Cu(HS)_2^-$, $Cu(HS)H_2S^0$ or $Cu(HS)(H_2O)^0$ complexes (Etschmann et al., 2010). The Cu K-edge XAFS spectra for aqueous linear Cu complexes (LCC) such as these have a very characteristic spectrum that displays a strong, rising resonance peak at \sim 8983 - 8984 eV (spectra labeled Structure L_a and L_b in Fig. 1 a, from Fulton et al., 2000a,b). Spectral differences are noted between different aqueous LCC species measured in these studies, primarily

reflected by very small shifts in the energy and intensity of the first resonance peak, but these tend to be small and difficult to quantify broadly using conventional XAFS techniques. Overall, these spectra are broadly similar and distinct from the spectra for Cu(I) species measured in simple oxides, such as Cu₂O (cuprite), which display a somewhat similar spectrum but with a first primary peak that is of notably lower intensity and clearly shifted to lower energies (Fig. 1a). These complexes are also distinct from octahedrally coordinated aqueous Cu(II) species, which have XAFS spectra shifted to much higher energy with an absorption maximum (white line) near 9000 eV (spectra labeled Structure O in Fig. 1 a, from Fulton et al., 2000a,b), similar to what is measured in crystalline Cu(II) compounds such as CuSO₄ and CuO.

It is worth noting that many of these observations are based largely on analysis of crystalline reference compounds and that, in glasses, increased lattice disorder is to be expected. Increased structural disorder surrounding the Cu atom is likely to result in subtle broadening of observed spectral features in what otherwise would be equivalent species. However, any significant changes that occur in the speciation of Cu within natural glasses should be readily discernable using XAFS and a robust first order characterization of the likely species present can be accomplished through comparison of spectra measured in natural glasses to those measured in crystalline and aqueous Cu-bearing standards. Although it is to be expected that the XAFS measured for Cu-bearing aqueous solutions and silicate glasses will be less structured than that measured in crystalline Cu compounds, due to decreased ordering of the former, differences in overall peak intensities and energy positions tend to be small.

3.2 Copper Speciation measured in 1 Atmosphere Experimental Basaltic Glasses

Cu K-edge XAFS spectra were measured in experimental glasses synthesized from Kīlauea basalt (Kīlauea tholeiite, Dufresne et al., 2009) and MORB (NMNH 118279, Cottrell et al., 2009) at various fO_2 values from NNO-4.2 to NNO+4.7. The experimental melts degassed during synthesis of these glasses, leading to S- and Cl-poor compositions. Four representative Cu-K-edge XAFS spectra from these glasses are presented in Fig. 2, showing spectra from glasses synthesized at fO_2 's between NNO-3.3 and NNO+4.7 in each of the two compositional suites. The Cu XAFS measured in these glasses have

absorption edges consistent with the presence of Cu¹⁺ species, across ~ 9 log units of fO₂. All absorption edges are ~2 eV lower than what is measured for Cu²⁺ species, with no divalent Cu being detectable. The measured spectra are indistinguishable from each other and similar to standard spectra measured for aqueous Cu⁺¹ linear complexes (LCC). Given that S and Cl were extensively degassed during the synthesis of these 1 atm experimental glasses, it is most likely that the XAFS reflects the presence of Cu-O ligands, possibly in a linear geometry. However, the XAFS spectral differences between Cu-O, Cu-Cl and Cu-S LCC species are subtle and challenging to distinguish using conventional XAFS analysis (Fulton et al., 2000a; Fulton et al., 2000b; Brugger et al., 2007; Etschmann et al., 2010). Nonetheless, the similarity in the measured Cu XAFS spectra for these experimental glasses equilibrated under grossly different redox conditions suggests that Cu readily complexes as a Cu-O species in S-poor basaltic melts.

3.3 Copper Speciation in Natural Volcanic Glasses

When comparing the Cu K-edge XAFS of natural basaltic glasses, a clear difference in speciation is observed that appears to directly correlate with dissolved S concentration. The spectra shown in Fig. 1b present an initial, comparative survey of natural glasses sampled from five different volcanic systems where melts equilibrated nominally at fO_2 < NNO. At these relatively reduced fO_2 conditions, S in the melts will be predominately present as sulfide species (Wallace and Carmichael, 1994; Jugo, 2009).

The Cu XAFS presented in Fig. 1b are separated into two groups based on observed spectroscopic differences. The group shown at the bottom of Fig. 1b are XAFS spectra collected from East Pacific Rise (described in Lanzirotti et al., 2018) and Juan de Fuca Ridge (NMNH VG-2, Jarosewich, 2002) MORB glasses and from olivine-hosted MI from Nyamuragira volcano (Head et al., 2011b; Head et al., 2018). The measured Cu XAFS for any individual sample is highly reproducible. As an example, Fig. 3 (right) shows 11 microfocused spectra (labeled "EPR pillow basalt") measured from the East Pacific Rise sample, collected at varying increments through the glassy zone of a sectioned pillow basalt, extending ~ 5.5 mm inwards from the quenched outer surface. To minimize the potential contribution of microlites to the measured XAFS spectra, the analytical points were chosen on the basis of XRF compositional

mapping. Within analytical uncertainty, these 11 spectra are indistinguishable across the rapidly cooled margin to the more slowly cooled interior glassy regions. This illustrates the homogeneity in Cu speciation that is observed in volcanic glasses and also shows that quench rates have no measurable impact on the coordination geometry and oxidation state of Cu. These Cu XAFS, measured in MORB and alkaline basalt glasses with S concentrations >1000 ppm, are well-matched by spectra measured in crystalline CuS (covellite) standards, with a rising absorption edge at ~ 1 eV higher energy than what is found in other Cu(I) species (Fig. 1a). Spectral features observed in the CuS model compound are subtly sharper than what is observed in the basaltic glasses, but this is consistent with the more ordered crystalline structure surrounding the Cu atoms in the model compound as compared to the glasses. This leads us to conclude that in these glasses Cu is complexed predominantly as a Cu(I) sulfide species, similar to what is observed in other covalently-bonded copper sulfides.

The second group of Cu XAFS, shown at the top of Fig. 1b, were measured in basaltic matrix glasses where S concentrations are less than 500 ppm. In contrast to what is observed in high-S glasses, these yield XAFS spectra that are most similar to spectra measured for aqueous linear Cu(I) complexes (LCC) and essentially indistinguishable from the spectra measured in 1 atm experimental glasses, where S abundances were low and presumably almost entirely lost to degassing. These low-S natural samples include fresh basaltic glass collected from the 1965 Makaopuhi Lava Lake at Kīlauea, Hawai'i (NMNH A-99, Jarosewich, 2002), matrix glasses sampled from a 2014 active lava flow at Kīlauea (described in Lanzirotti et al., 2018), and matrix glass in a sample of lapilli from a 2015 eruption at Mt. Etna, Italy (Pompilio et al., 2017). The low S content in all these glasses is most likely due to degassing of S during melt decompression and eruption. Similar to what is observed in the 1 atm experimental glasses, we hypothesize that the Cu speciation in these natural low-S glasses most likely reflects the presence of Cu¹⁺-O ligands.

To better understand this observed transition from oxygen- to sulfur-bound Cu species in natural systems, Cu speciation was also measured in MI and matrix glasses in samples collected from the 2008-2018 Kīlauea summit eruptions at Halema'uma'u in Hawai'i (Thornber et al., 2015; Neal et al., 2018).

Olivine-hosted melt inclusions (n=71) and surrounding matrix glass (n=18) from materials erupted during 2008-2018 were analyzed for Cu K-edge XAFS as well as for S and Cu abundance. This sequence of samples provides a unique opportunity to systematically evaluate how changes in Cu speciation correlate with magmatic S content. Thornber et al. (2015) showed that olivine-hosted MI sampled at Kīlauea summit between 2008 and 2014 present a broad range in S concentration from <450 ppm to >1000 ppm. The observed variations in S abundance tend to be fairly systematic, with the highest S concentrations generally occurring in the earliest erupted MI from this sequence. Kīlauea's 2018 fissure eruption in the lower ERZ marks a major change in volcanic activity, and MI in tephra from this eruption have a wide range of S contents (~ 600–1100 ppm S), departing from the previous general temporal trend of decreasing S. It should be noted that whereas Kīlauea lava compositions are consistent with equilibration at fO_2 < NNO (Carmichael and Ghiorso, 1990), studies have shown that progressive S degassing of these melts does impact the melt oxidation state to a small degree, particularly reflected by reduction of iron (Moussallam et al., 2016; Helz et al., 2017).

Calculated S concentrations at sulfide saturation (SCSS calculated using Fortin et al., 2015 and Smythe et al., 2017 models, assuming 1160°C and Δ NNO-1) for the 2008-2013 suite of Kīlauea glasses (Thornber et al., 2015) average between \sim 1350-1500 ppm S, which is consistent with previously calculated SCSS abundances for Kīlauea tholeiite (Wallace and Anderson Jr., 1998). Sulfur concentrations in Kīlauea MI range from \sim 50–1360 ppm S, thus, the majority of the MI glasses analyzed here from Kīlauea preserve melt S contents that are below sulfide saturation.

Kīlauea MI with measured S abundances >1000 ppm yield Cu XAFS spectra similar to spectra measured for CuS (Fig. 4a) and similar to what is measured in other high-S magmatic glasses (i.e. MORB and Nyamuragira alkaline basaltic glasses). The Kīlauea matrix glasses (Fig. 4a,b,c) and MI (Fig. 4c) with S abundances <500 ppm yield Cu XAFS spectra (Fig. 4) that are similar to what has been measured in 1 atm experimental glasses, most likely indicating the dominance of linearly complexed Cu(I)-oxide species. This is, again, consistent with what is observed for other low-S volcanic glasses analyzed and shown in Fig. 1b. Kīlauea MI with intermediate S abundances, between 500-1000 ppm, yield spectra

consistent with the presence of both Cu species (Fig. 4b). These intermediate-type spectra can be quantitatively reproduced using a two-component linear mixing model (Fig. 5, Table 1) of end-member Cu(I)-sulfide (using covellite CuS spectra) and Cu(I)-oxide (using 1 atm experimental Kīlauea tholeiite glass) species. The linear combination fit (LCF) modeling shows that the degree of mixing between Cu(I)-sulfide and Cu(I)-oxide species is highly correlated with measured S abundance in the glass (Fig. 6), particularly between 500-1000 ppm S, whereas no discernable correlation is observed between Cu speciation and dissolved Cu concentration in the glasses (Fig. 7). Although the lowest fraction of either end-member species calculated in the LCF modeling is ~ 5% (Table 1), overall the modeling suggests that ~ 20% of the minor species persists at the highest and lower S abundances measured (Fig. 6). This interpretation does assume that the Cu(I)-oxide and Cu(I)-sulfide end-members chosen for modeling are well-representative of species found in the natural samples. For example, it is noted that the spectrum for the CuS model compound appear slightly more ordered than the spectra measured in these glasses. However, the *R-factors* for the LCF fitting are all smaller than 0.008, suggesting that these two components model the observed spectra very well, with uncertainties of only a few percent.

4. Discussion

The results of this study indicate that, in natural basaltic melts equilibrated at fO2's below NNO, two distinct Cu species are observed as chemical components in the melt. Both species are shown to coexist in the natural systems studied, with the relative proportions largely controlled by the availability of S. In basaltic systems with S concentrations > 1000 ppm, Cu(I)-sulfide species dominate, identified by XAFS spectra that are consistent with what is observed in largely covalently-bonded CuS model compounds. By contrast, in basaltic systems with S concentrations <500 ppm, linear Cu(I) species appear to dominate. The similarity between XAFS spectra measured in low-S natural glasses and in S-free experimental glasses suggests it is likely these are linearly-complexed Cu(I)-oxide species. At intermediate S concentrations, the spectra can be well-modeled as mixtures of these two distinct Cu(I)-oxide and -sulfide species, with no clear evidence of the stabilization of an intermediate Cu-oxysulfide species. It is possible

that some of the Cu atoms in the linear complexes measured are bound to ligands other than O (i.e., S or Cl). However, XAFS measurements of Cu(I)-S and Cu(I)-Cl linear complexes in hydrothermal experiments (Fulton et al., 2000a; Fulton et al., 2000b; Brugger et al., 2007; Etschmann et al., 2010) show that such compounds are likely to yield XAFS spectra that would be difficult to distinguish spectroscopically from linearly complexed Cu(I)-O species. In contrast, the XAFS spectra measured in high-S glasses are distinct from what we interpret to be Cu(I)-oxide spectra and, again, consistent with the presence of a largely covalently-bonded Cu(I)-sulfide. The LCF modeling conducted as part of this study also suggests that both species persist throughout the range of S abundances measured in the natural glasses studied here. Thus, even in strongly degassed melts where S concentrations are typically less than 500 ppm, as much as 20% of Cu may continue to be complexed as Cu-S ligands. In our Kīlauea data, there is no apparent loss of Cu from the melt during the strong degassing of S that occurs at low pressure. This may reflect the fact that Cu can readily complex with oxygen as the availability of S ligands in the melt decreases. This could in turn help to explain why Cu fluxes in volcanic gases from low-fO2 basaltic volcanoes such as Kīlauea are relatively low (e.g., Edmonds et al., 2018).

Based on the XAFS results, the relationship between dissolved Cu species in the melt can be described by the following equilibrium:

$$CuO_{0.5}^m + \frac{1}{4}S_2^m = CuS_{0.5}^m + \frac{1}{4}O_2^m$$
 (1)

where $CuO_{0.5}^m$ represents the presence of Cu(I)-oxide linear complexes in the melt phase and $CuS_{0.5}^m$ represents the presence Cu(I)-sulfide complexes. Such an equilibrium illustrates how the Cu complexation in the melt phases is dependent on both fO_2 and fS_2 and hence the dissolved S content in the melt. Although a number of experimental studies using sulfide-saturated basaltic melt compositions have shown that fO_2 can exert a strong control on Cu solubility and partitioning (Peach and Mathez, 1993; Gaetani and Grove, 1997; Holzheid and Lodders, 2001; Ripley et al., 2002; Zajacz et al., 2012), many of these studies have also noted an apparent weaker correlation between Cu solubility and melt S²⁻ concentration (Ripley and Brophy, 1995; Ripley et al., 2002; Zajacz et al., 2012). This has led to

speculations that some degree of Cu-S complexing occurs in basaltic melts when S contents are elevated.

The results presented here are consistent with these hypotheses.

431

432

433

434

435

436

437

438

439

440

441

442

443

444

445

446

447

448

449

450

451

452

453

454

The dominance of $CuS_{0.5}^m$ species at high melt S contents is also useful for constraining possible heterogeneous equilibria that describe the transfer of Cu and S between the melt phase and precipitating sulfides at sulfide saturation conditions. For example, in the presence of an iron sulfide phase, hypothetical reactions such as:

$$CuS_{0.5}^{m} + FeS^{po} + \frac{1}{4}S_{2}^{m} = CuFeS_{2}^{iss}$$
 (2)

where po is pyrrhotite and iss is intermediate solid solution, would be more accurately descriptive based on the observed speciation. This reaction does not explicitly depend on fO₂ and thus could explain the experimental observation that Cu partitioning into intermediate solid solution is less strongly affected by fO₂ than would be expected if Cu complexing with O in the silicate melt was the dominant solution mechanism for Cu (Ripley and Brophy, 1995; Ripley et al., 2002). It is worth noting that the majority of tholeiitic magmas equilibrated at fO_2 's < NNO will be expected to contain on the order of 800-1000 ppm dissolved sulfur (unless or until they are affected by near-surface degassing) at <~22% partial melting of the source (Ding and Dasgupta, 2017). These are conditions relevant broadly to mantle-derived melts. Given that the results presented here show that Cu-O complexes only occur, or are only significant, when S degassing has largely removed S from the melt, it should be expected that melts at depth will have Cu strongly complexed with S. Therefore, melts at depth are likely to have Cu strongly complexed with S, with Cu-O complexes only likely to be present in significant amounts when S degassing has removed S from the melt. Additional planned studies will also seek to understand how Cu speciation changes in melts equilibrated at fO₂'s > NNO, where sulfate begins to be the dominant S species in the liquid (Jugo, 2009; Beermann et al., 2011). At these redox conditions, the sulfur solubility of the melt increases significantly as the dominant sulfur species changes from S²⁻ to S⁶⁺ with increasing fO₂. These are redox conditions

particularly relevant to arc magmatic systems, where the majority of porphyry copper deposits form. It

has been hypothesized that the significantly higher sulfur solubility of these oxidized systems (Carroll and Rutherford, 1985; Jugo, 2009) may promote Cu enrichment in the evolving silicate melt. Although the results of this study would suggest that Cu-S species should be favored in the presence of high magmatic S, this likely requires the availability of S²⁻ ions in the silicate liquid. Previous studies have hypothesized that Cu mineralization in such melts should primarily be controlled by the availability of reduced sulfur, S²⁻, given that Cu ore minerals are largely sulfides. Reduction of sulfate in oxidized magmas has been suggested as a mechanism for promoting deposition, possibly due to ferrous iron oxidation during magnetite and hematite crystallization (Sun et al., 2013; Zhang et al., 2017). The speciation of dissolved Cu in the melt prior to sulfate reduction remains unclear, however. In the presence of S⁶⁺ it may be more favorable for Cu to complex as either oxide or sulfate species, and our XAFS results show that Cu-oxide species can be stabilized. It is interesting to note that in experiments in which Cu activity was fixed by equilibrium with a AuCu metal alloy capsule, Cu solubilities show a strong increase at fO₂ increases.

5. Conclusions

This study presents Cu K-edge XAFS measurements from natural magmatic glasses, as a means of evaluating Cu speciation in sulfide-dominated basaltic magmas equilibrated below the nickel – nickel oxide (NNO) redox buffer. Results from several volcanic systems, including spectra measured from MORB glasses and MI and matrix glasses from Mt. Etna, Nyamuragira, and Kīlauea volcanoes, are consistent in showing that both Cu(I)-sulfide species and linearly complexed Cu(I)-oxide species are stabilized in natural systems. In some cases, both species are found to coexist, with the proportions being highly correlated with measured S abundance in the glasses. Spectra measured in olivine-hosted melt inclusions from recent Kīlauea volcanics show that Cu in these glasses is strongly complexed as Cu(I)-sulfide when S concentrations exceed 1000 ppm. Below 1000 ppm S, oxygen complexing begins to be observed and dominates at S concentrations below 500 ppm, although Cu remains complexed to both O-and S-ligands at the lowest S abundances measured. How these observed changes in Cu speciation impact

metal solubility remain unclear and will require further study. However, it is clear that both oxide and sulfide complexing of Cu in silicate melts should be expected and that changes in S content of the melt, for example through volatile degassing or incorporation of externally derived sulfur to the magma, can lead to direct changes in the stabilized Cu species. Insomuch as species complexing is important for partitioning behavior in magmas, the results presented here suggest that the partitioning behavior of Cu into sulfide melts, solids (Cu-sulfide), and fluids (vapor phase and Cu-chloride brines) may be significantly different depending on the S content of the melt. These observations, therefore, provide guidance for the design of future experimental work on Cu-partitioning behavior, where the sulfur content of the melt needs to be a carefully controlled parameter in order to constrain and stabilize Cu-speciation...

Acknowledgements

This study was funded by a National Science Foundation Earth Sciences collaborative research grant to A. Lanzirotti, E. Head, M. McCanta and P. Wallace (EAR- 1834930, 1834941, 1834959, 1834939). A. Lerner acknowledges support from the National Science Foundation Graduate Research Fellowship Program under grant #1309047. XAFS spectroscopy data were collected at GeoSoilEnviroCARS (Sector 13), Advanced Photon Source (APS), Argonne National Laboratory. GeoSoilEnviroCARS is supported by the National Science Foundation, Earth Sciences (EAR-1128799) and Department of Energy, Geosciences (DE-FG02-94ER14466). Use of the Advanced Photon Source was supported by the U.S. Department of Energy, Office of Science, Office of Basic Energy Sciences, under contract no. DE-AC02-06CH11357. We acknowledge the Smithsonian Institute National Museum of Natural History Department of Mineral Sciences for the use of NMNH 117393 basalt reference glasses for this study and for providing samples of basaltic glass standards VG-2 (NMNH 111240-52) and A-99 (NMNH 113498-1). We wish to thank Dr. Penny King for use of standard glasses synthesized for the Dufresne et al. (2009) study. The USGS and S. Wilson are thanked for providing glass reference standards GSA-1G, GSC-1G, GSD-1G, GSE-1G and BCR-2G. We thank Dr. Massimo Pompilio at the Instituto Nazionale di Geofisica e Vulcanologia for providing samples from Mt. Etna for study. We thank Dr. Barbara Etschmann, Dr.

Joel Brugger and Dr. John Fulton for providing us standard spectra from their earlier studies for comparison. Dr. John Mavrogenes is thanked for discussions in preparing this manuscript. We also wish the thank the very constructive reviews by Ed Ripley and two anonymous reviewers, as well as comments from Associate Editor Weidong Sun, which greatly improved the final version of this manuscript. References Beermann O., Botcharnikov R. E., Holtz F., Diedrich O. and Nowak M. (2011) Temperature dependence of sulfide and sulfate solubility in olivine-saturated basaltic magmas. Geochim. Cosmochim. Acta **75**, 7612–7631. Brounce M., Kelley K. A., Cottrell E. and Reagan M. K. (2015) Temporal evolution of mantle wedge oxygen fugacity during subduction initiation. Geology 43, 775–778. Brugger J., Etschmann B., Liu W., Testemale D., Hazemann J.-L., Emerich H., Van Beek W. and Proux O. (2007) An XAS study of the structure and thermodynamics of Cu (I) chloride complexes in brines up to high temperature (400 C, 600bar). Geochim. Cosmochim. Acta 71, 4920–4941. Candela P. A. and Holland H. D. (1984) The partitioning of copper and molybdenum between silicate melts and aqueous fluids. Geochim. Cosmochim. Acta 48, 373–380. Carmichael I. S. and Ghiorso M. S. (1990) The effect of oxygen fugacity on the redox state of natural liquids and their crystallizing phases. Rev. Mineral. Geochem. 24, 191–212. Carroll M. R. and Rutherford M. J. (1985) Sulfide and sulfate saturation in hydrous silicate melts. J. Geophys. Res. Solid Earth 1978–2012 90, C601–C612. Cottrell E., Kelley K. A., Lanzirotti A. and Fischer R. A. (2009) High-precision determination of iron oxidation state in silicate glasses using XANES. Chem. Geol. 268, 167–179. Criss J. W., Birks L. S. and Gilfrich J. V. (1978) Versatile x-ray analysis program combining fundamental

parameters and empirical coefficients. Anal. Chem. 50, 33–37.

505

506

507

508

509

510

511

512

513

514

515

516

517

518

519

520

521

522

523

524

525

526

527

528	Danyushevsky L. V., McNeill A. W. and Sobolev A. V. (2002) Experimental and petrological studies of
529	melt inclusions in phenocrysts from mantle-derived magmas: an overview of techniques,
530	advantages and complications. Chem. Geol. 183, 5-24.
531	Ding S. and Dasgupta R. (2017) The fate of sulfide during decompression melting of peridotite-
532	implications for sulfur inventory of the MORB-source depleted upper mantle. Earth Planet. Sci.
533	Lett. 459, 183–195.
534	Dufresne C. D., King P. L., Dyar M. D. and Dalby K. N. (2009) Effect of SiO ₂ , total FeO, Fe ³⁺ /Fe ²⁺ , and
535	alkali elements in basaltic glasses on mid-infrared. Am. Mineral. 94, 1580–1590.
536	Edmonds M., Mather T. A. and Liu E. J. (2018) A distinct metal fingerprint in arc volcanic emissions.
537	Nat. Geosci. 11, 790.
538	Etschmann B. E., Liu W., Testemale D., Mueller H., Rae N. A., Proux O., Hazemann JL. and Brugger J.
539	(2010) An in situ XAS study of copper (I) transport as hydrosulfide complexes in hydrothermal
540	solutions (25-592 C, 180-600bar): speciation and solubility in vapor and liquid phases. Geochim.
541	Cosmochim. Acta 74 , 4723–4739.
542	Fellows S. A. and Canil D. (2012) Experimental study of the partitioning of Cu during partial melting of
543	Earth's mantle. Earth Planet. Sci. Lett. 337, 133–143.
544	Fornari D. J., Von Damm K. L., Bryce J. G., Cowen J. P., Ferrini V., Fundis A., Lilley M. D., Luther III
545	G. W., Mullineaux L. S. and Perfit M. R. (2012) The East Pacific Rise between 9 N and 10 N:
546	Twenty-five years of integrated, multidisciplinary oceanic spreading center studies.
547	Oceanography 25, 18–43.
548	Fortin MA., Riddle J., Desjardins-Langlais Y. and Baker D. R. (2015) The effect of water on the sulfur
549	concentration at sulfide saturation (SCSS) in natural melts. Geochim. Cosmochim. Acta 160, 100-
550	116.
551	Fulton J. L., Hoffmann M. M. and Darab J. G. (2000a) An X-ray absorption fine structure study of copper
552	(I) chloride coordination structure in water up to 325 C. Chem. Phys. Lett. 330, 300-308.

553	Fulton J. L., Hoffmann M. M., Darab J. G., Palmer B. J. and Stern E. A. (2000b) Copper (I) and copper
554	(II) coordination structure under hydrothermal conditions at 325 C: an X-ray absorption fine
555	structure and molecular dynamics study. J. Phys. Chem. A 104, 11651-11663.
556	Gaetani G. A. and Grove T. L. (1997) Partitioning of moderately siderophile elements among olivine,
557	silicate melt, and sulfide melt: constraints on core formation in the Earth and Mars. Geochim.
558	Cosmochim. Acta 61 , 1829–1846.
559	Goh S. W., Buckley A. N., Lamb R. N., Rosenberg R. A. and Moran D. (2006) The oxidation states of
560	copper and iron in mineral sulfides, and the oxides formed on initial exposure of chalcopyrite and
561	bornite to air. Geochim. Cosmochim. Acta 70, 2210–2228.
562	Head E., Lanzirotti A., Newville M. and Sutton S. (2018) Vanadium, Sulfur, and Iron Valences in Melt
563	Inclusions as a Window into Magmatic Processes: A Case Study at Nyamuragira Volcano,
564	Africa. Geochim. Cosmochim. Acta 226, 149–173.
565	Head E. M., Shaw A. M., Wallace P. J., Sims K. W. and Carn S. A. (2011a) Insight into volatile behavior
566	at Nyamuragira volcano (DR Congo, Africa) through olivine-hosted melt inclusions. Geochem.
567	Geophys. Geosystems 12, 1–22.
568	Head E. M., Shaw A. M., Wallace P. J., Sims K. W. and Carn S. A. (2011b) Insight into volatile behavior
569	at Nyamuragira volcano (DR Congo, Africa) through olivine-hosted melt inclusions. Geochem.
570	Geophys. Geosystems 12, 1–22.
571	Helz R. T., Cottrell E., Brounce M. N. and Kelley K. A. (2017) Olivine-melt relationships and
572	syneruptive redox variations in the 1959 eruption of Kīlauea Volcano as revealed by XANES. J.
573	Volcanol. Geotherm. Res. 333–334 , 1–14.
574	Holloway J. R. and Burnham C. W. (1972) Melting Relations of Basalt with Equilibrium Water Pressure
575	Less Than Total Pressure. J. Petrol. 13, 1–29.
576	Holzheid A. and Lodders K. (2001) Solubility of copper in silicate melts as function of oxygen and sulfur
577	fugacities, temperature, and silicate composition. Geochim. Cosmochim. Acta 65, 1933–1951.

578	Imai A., Listanco E. L. and Fujii T. (1993) Petrologic and sulfur isotopic significance of highly oxidized
579	and sulfur-rich magma of Mt. Pinatubo, Philippines. Geology 21, 699-702.
580	Jarosewich E. (2002) Smithsonian Microbeam Standards. J. Res. Natl. Inst. Stand. Technol. 107, 681-
581	685.
582	Jenner F. E. and O'Neill H. S. C. (2012) Major and trace analysis of basaltic glasses by laser-ablation
583	ICP-MS. Geochem. Geophys. Geosystems 13(3).
584	Jochum K. P., Willbold M., Raczek I., Stoll B. and Herwig K. (2005) Chemical Characterisation of the
585	USGS Reference Glasses GSA-1G, GSC-1G, GSD-1G, GSE-1G, BCR-2G, BHVO-2G and BIR-
586	1G Using EPMA, ID-TIMS, ID-ICP-MS and LA-ICP-MS. Geostand. Geoanalytical Res. 29,
587	285–302.
588	Jugo P. J. (2009) Sulfur content at sulfide saturation in oxidized magmas. <i>Geology</i> 37, 415–418.
589	Jugo P. J., Candela P. A. and Piccoli P. M. (1999) Magmatic sulfides and Au:Cu ratios in porphyry
590	deposits: an experimental study of copper and gold partitioning at 850°C, 100 MPa in a
591	haplogranitic melt-pyrrhotite-intermediate solid solution-gold metal assemblage, at gas
592	saturation. <i>Lithos</i> 46 , 573–589.
593	Kau L. S., Spira-Solomon D. J., Penner-Hahn J. E., Hodgson K. O. and Solomon E. I. (1987) X-ray
594	absorption edge determination of the oxidation state and coordination number of copper.
595	Application to the type 3 site in Rhus vernicifera laccase and its reaction with oxygen. J. Am.
596	Chem. Soc. 109, 6433–6442.
597	Kelley K. A. and Cottrell E. (2009) Water and the oxidation state of subduction zone magmas. Science
598	325 , 605–607.
599	Kiseeva E. S. and Wood B. J. (2013) A simple model for chalcophile element partitioning between
600	sulphide and silicate liquids with geochemical applications. Earth Planet. Sci. Lett. 383, 68-81.
601	Kraft S., Stümpel J., Becker P. and Kuetgens U. (1996) High resolution x-ray absorption spectroscopy
602	with absolute energy calibration for the determination of absorption edge energies. Rev. Sci.
603	Instrum. 67, 681–687.

604	Lanzirotti A., Dyar M. D., Sutton S., Newville M., Head E., Carey C. J., Mccanta M., Lee L., King P. L.
605	and Jones J. (2018) Accurate predictions of microscale oxygen barometry in basaltic glasses
606	using V K-edge X-ray absorption spectroscopy: A multivariate approach. Am. Mineral. 103,
607	1282–1297.
608	Lanzirotti A., Sutton S. R., Flynn G. J., Newville M. and Rao W. (2008) Chemical composition and
609	heterogeneity of Wild 2 cometary particles determined by synchrotron X-ray fluorescence.
610	Meteorit. Planet. Sci. 43, 187–213.
611	Lanzirotti A., Tappero R. and Schulze D. G. (2010) Practical applications of synchrotron-based hard X-
612	ray microprobes in the soil sciences. In Grafe, M. and Singh, B. (eds.), Practical Application of
613	Synchrotron-Based Hard X-Ray Microprobes in Soil Sciences, Synchrotron-based Techniques in
614	Soils and Sediments 34, 27-72, Elsevier, Oxford
615	Lee CT. A., Luffi P., Chin E. J., Bouchet R., Dasgupta R., Morton D. M., Le Roux V., Yin Q. and Jin D.
616	(2012) Copper systematics in arc magmas and implications for crust-mantle differentiation.
617	Science 336 , 64–68.
618	Li Y. and Audétat A. (2012) Partitioning of V, Mn, Co, Ni, Cu, Zn, As, Mo, Ag, Sn, Sb, W, Au, Pb, and
619	Bi between sulfide phases and hydrous basanite melt at upper mantle conditions. Earth Planet.
620	Sci. Lett. 355 , 327–340.
621	Marescotti P., Vanko D. A. and Cabella R. (2000) From oxidizing to reducing alteration: Mineralogical
622	variations in pillow basalts from the east flank, Juan de Fuca Ridge. In Proc. Ocean Drill.
623	Program Sci. Results pp. 119–136.
624	Métrich N. and Wallace P. J. (2008) Volatile abundances in basaltic magmas and their degassing paths
625	tracked by melt inclusions. Rev. Mineral. Geochem. 69, 363-402.
626	Moussallam Y., Edmonds M., Scaillet B., Peters N., Gennaro E., Sides I. and Oppenheimer C. (2016) The
627	impact of degassing on the oxidation state of basaltic magmas: A case study of Kīlauea volcano.
628	Earth Planet. Sci. Lett. 450 , 317–325.

- Neal C. A., Brantley S. R., Antolik L., Babb J., Burgess M., Calles K., Cappos M., Chang J. C., Conway
- S., Desmither L., Dotray P., Elias T., Fukunaga P., Fuke S., Johanson I. A., Kamibayashi K.,
- Kauahikaua J., Lee R. L., Pekalib S., Miklius A., Million W., Moniz C. J., Nadeau P. A., Okubo
- P., Parcheta C., Patrick M. P., Shiro B., Swanson D. A., Tollett W., Trusdell F., Younger E. F.,
- Zoeller M. H., Montgomery-Brown E. K., Anderson K. R., Poland M. P., Ball J., Bard J.,
- 634 Coombs M., Dietterich H. R., Kern C., Thelen W. A., Cervelli P. F., Orr T., Houghton B. F.,
- Gansecki C., Hazlett R., Lundgren P., Diefenbach A. K., Lerner A. H., Waite G., Kelly P., Clor
- L., Werner C., Mulliken K. and Fisher G. (2018) The 2018 rift eruption and summit collapse of
- 637 Kīlauea Volcano. *Science* **363**, 367-374.
- 638 Newville M. (2013) Larch: An Analysis Package for XAFS and Related Spectroscopies. J. Phys. Conf.
- 639 Ser. **430**, 012007.
- Pattrick R., Mosselmans J., Charnock J., England K., Helz G., Garner C. and Vaughan D. (1997) The
- structure of amorphous copper sulfide precipitates: An X-ray absorption study. *Geochim.*
- 642 *Cosmochim. Acta* **61**, 2023–2036.
- Peach C. L. and Mathez E. A. (1993) Sulfide melt-silicate melt distribution coefficients for nickel and
- iron and implications for the distribution of other chalcophile elements. *Geochim. Cosmochim.*
- 645 *Acta* **57**, 3013–3021.
- Poland M., Miklius A., Orr T., Sutton J., Thornber C. and Wilson D. (2008) New episodes of volcanism
- at Kilauea Volcano, Hawaii. Eos Trans. Am. Geophys. Union 89, 37–38.
- Pompilio M., Bertagnini A., Carlo P. D. and Roberto A. D. (2017) Magma dynamics within a basaltic
- conduit revealed by textural and compositional features of erupted ash: the December 2015 Mt.
- Etna paroxysms. Sci. Rep. 7, 4805.
- Prinz M. (1967) Geochemistry of basaltic rocks: trace elements. In. *Basalts* 1, 271–333.
- Ravel B. and Newville M. (2005) ATHENA, ARTEMIS, HEPHAESTUS: data analysis for X-ray
- absorption spectroscopy using IFEFFIT. J. Synchrotron Radiat. 12, 537–541.

- Ripley E. M. and Brophy J. G. (1995) Solubility of copper in a sulfur-free mafic melt. *Geochim*.
- 655 *Cosmochim. Acta* **59**, 5027–5030.
- Ripley E. M., Brophy J. G. and Li C. (2002) Copper solubility in a basaltic melt and sulfide liquid/silicate
- melt partition coefficients of Cu and Fe. *Geochim. Cosmochim. Acta* **66**, 2791–2800.
- 658 Sillitoe R. H. (1997) Characteristics and controls of the largest porphyry copper-gold and epithermal gold
- deposits in the circum-Pacific region. Aust. J. Earth Sci. 44, 373–388.
- 660 Sillitoe R. H. (2010) Porphyry Copper Systems. Econ. Geol. 105, 3–41.
- 661 Smythe D. J., Wood B. J. and Kiseeva E. S. (2017) The S content of silicate melts at sulfide saturation:
- New experiments and a model incorporating the effects of sulfide composition. *Am. Mineral.* **102**,
- 663 795–803.
- Sun W., Arculus R. J., Bennett V. C., Eggins S. M. and Binns R. A. (2003) Evidence for rhenium
- 665 enrichment in the mantle wedge from submarine arc–like volcanic glasses (Papua New Guinea).
- *Geology* **31**, 845–848.
- 667 Sun W., Liang H., Ling M., Zhan M., Ding X., Zhang H., Yang X., Li Y., Ireland T. R. and Wei Q.
- 668 (2013) The link between reduced porphyry copper deposits and oxidized magmas. *Geochim*.
- 669 *Cosmochim. Acta* **103**, 263–275.
- Sutton S. R., Bertsch P. M., Newville M., Rivers M., Lanzirotti A. and Eng P. (2002) Microfluorescence
- and Microtomography Analyses of Heterogeneous Earth and Environmental Materials. *Rev.*
- 672 *Mineral. Geochem.* **49**, 429–483.
- Thornber C. R., Orr T. R., Heliker C. and Hoblitt R. P. (2015) Petrologic testament to changes in shallow
- magma storage and transport during 30+ years of recharge and eruption at Kılauea Volcano,
- Hawai 'i. Hawaii. Volcanoes Source Surf. 208, 147.
- Vegelius J. R., Kvashnina K. O., Hollmark H., Klintenberg M., Kvashnin Y. O., Soroka I. L., Werme L.
- and Butorin S. M. (2012) X-ray Spectroscopic Study of Cu₂S, CuS, and Copper Films Exposed to
- 678 Na₂S Solutions. J. Phys. Chem. C 116, 22293–22300.

679	Vigneresse JL., Truche L. and Chattaraj P. K. (2014) Metal (copper) segregation in magmas. Lithos 208,
680	462–470.
681	Wallace P. and Carmichael I. S. E. (1992) Sulfur in basaltic magmas. Geochim. Cosmochim. Acta 56,
682	1863–1874.
683	Wallace P. J. and Anderson Jr. A. T. (1998) Effects of eruption and lava drainback on the H2O contents
684	of basaltic magmas at Kilauea Volcano. Bull. Volcanol. 59, 327-344.
685	Wallace P. J. and Carmichael I. S. E. (1994) S speciation in submarine basaltic glasses as determined by
686	measurements of S Kalpha X-ray wavelength shifts. Am. Mineral. 79, 161-167.
687	Zajacz Z., Candela P. A., Piccoli P. M., Sanchez-Valle C. and Wälle M. (2013) Solubility and partitioning
688	behavior of Au, Cu, Ag and reduced S in magmas. Geochim. Cosmochim. Acta 112, 288-304.
689	Zajacz Z., Candela P. A., Piccoli P. M., Wälle M. and Sanchez-Valle C. (2012) Gold and copper in
690	volatile saturated mafic to intermediate magmas: Solubilities, partitioning, and implications for
691	ore deposit formation. Geochim. Cosmochim. Acta 91, 140-159.
692	Zhang C., Sun W., Wang J., Zhang L., Sun S. and Wu K. (2017) Oxygen fugacity and porphyry
693	mineralization: a zircon perspective of Dexing porphyry Cu deposit, China. Geochim.
694	Cosmochim. Acta 206 , 343–363.

Figure Captions

696

697

698

699

700

701

702

703

704

705

706

707

708

709

710

711

712

713

714

715

716

717

718

719

720

721

Figure 1: (a) Cu K-edge XAFS spectra collected for various Cu-bearing standard materials, intensities offset vertically for clarity. Spectra labeled Structure La, Lb and O are for aqueous Cu species from Fulton et al. (2000a,b), energy shifted so the calibration is consistent with what is used in this study. The L_a and L_b Cu(I) complexes (top two curves respectively) have a linear geometry with a strong spectral maximum at ~ 8983.5 eV (designated by a dashed vertical line marked LCC). Structure O complexes (bottom most curve) are Cu(II) species with an octahedral symmetry exhibiting a spectral maximum just below 9000 eV (dashed vertical line marked Type O). Spectra for CuS, Cu₂S, CuFeS₂, CuO, and Cu₂O crystalline compounds are also shown (all labeled accordingly). The first maximum in the CuS spectrum lies at ~ 8987 eV (dashed vertical line marked CuS). Cu₂O has a pre-edge peak similar to that observed in LCC, but at lower energy and intensity. (b) Cu K-edge XAFS spectra collected for natural magmatic glasses including (bottom) matrix glasses from MORB Juan de Fuca Ridge, MORB East Pacific Rise and Nyamuragira alkaline basalt and (top) matrix glasses from 1965 Kīlauea summit eruption, 2014 Kīlauea lava flow and in lapilli from a 2015 eruption at Mt. Etna. The two groups are offset vertically for clarity and labeled, respectively, *High-S glasses* and *Low-S glasses*.

Figure 2: Cu K-edge XAFS spectra measured in experimental glasses synthesized from Kīlauea basalt (Dufresne et al. 2009) and MORB (NMNH 118279, Cottrell et al. 2009) starting materials at various fO_2 from NNO-0.68 to NNO+4.7. These glass synthesis experiments were all conducted in S-free atmosphere and all preserve what appear to be predominantly LCC species, independent of fO_2 . The energies of spectral maxima for LCC and CuS standards are indicated by vertical dashed lines (see Fig. 1a).

Figure 3: Plane-light photomicrograph (left) and Cu K-edge XAFS spectra (right) from a sample of pillow basalt glass dredged from the East Pacific Rise. A 1 mm scale bar is shown in the lower left corner of the photomicrograph and the points selected for XAFS analysis are

annotated in yellow, extending ~ 5.5 mm into the pillow from its quenched surface (left side of the sample). Normalized Cu XAFS spectra for each analysis point are shown, and are indistinguishable throughout the pillow margin. Comparison spectra for CuS and experimental 1 atm Kīlauea tholeiitic basalt (NNO+4.7) offset vertically. The energies of spectral maxima for LCC and CuS standards are indicated by vertical dashed lines (see Fig. 1a).

Figure 4: Selected Cu K-edge XAFS spectra collected from Kīlauea summit MI (shown in blue) and matrix glasses (shown in red) erupted March 27, 2008 (top), September 17, 2009 (middle) and January 17, 2011 (bottom). Annotations on each figure show how many analyses are presented (designated *n*=) and measured S abundances for each glass. Uniformly, spectra collected in glasses with the highest measured S are most similar to spectra measured in crystalline CuS, while spectra from low S MI and matrix glasses are similar to that measured in aqueous LCC species, which we interpret as indicating the dominance of Cu¹⁺-O in these glasses. Spectra from the 2009 MI, which have intermediate S content, appear consistent with a two-component mixture of these two species. The energies of spectral maxima for LCC and CuS standards are indicated by vertical dashed lines (see Fig. 1a).

Figure 5: Examples of linear combination fits (LCF) of Kīlauea glass spectra used to determine the relative percentage of Cu(I)-oxide and -sulfide species in each analysis. Examples are shown for analyzed olivine-hosted MI erupted in 2008 (bottom) and 2014 (top). Measured edge-step normalized Cu XAFS spectra are shown as solid red curves and the predicted fit, using CuS model compound and experimental 1 atm Kīlauea tholeiitic (representing the Cu¹⁺-O component) as the predictor components, are shown as dashed blue curves. Also plotted are the weighted component spectra for the fit and the residual.

Figure 6: Plot of measured S abundance vs calculated % Cu¹⁺-O for analyzed Kīlauea glasses. The % Cu-oxide is calculated assuming a mixture of Cu¹⁺-O and Cu¹⁺-S on the basis of linear combination fitting of the measured Cu XAFS spectra, using spectra from CuS standard and

experimental 1 atm Kīlauea tholeiitic basalt as the predictor components. Matrix glasses are shown as triangles while MI are shown as open circles. Color-coding of the symbols indicates the date of eruption by year. Matrix glasses and MI with S abundances <500 ppm have spectra most consistent with what is measured for degassed, 1 atm experimental glasses while MI with S concentrations exceeding 1000 ppm are most similar to Cu XAFS spectra measured in CuS. MI with intermediate S concentrations appear consistent with a two-component mixture of these two species.

Figure 7: Plot of measured Cu vs S abundance for analyzed Kīlauea glasses. Symbol designations are the same as described for Fig. 6. Copper abundance is relatively uniform compared to the nearly two order-of-magnitude variation in S abundance.

Table 1: Kilauea glasses: sample information and calculated ppm S, ppm Cu, and % linear Cu complex

		MI			%	LCF
	Sampling	Diameter	S	Cu	Cu ¹⁺ -	R-Factor
Sample ID	Date ^a	(µm)	(ppm) ^b	(ppm) ^c	oxide ^d	(‰) ^e
KS08-11-MI1	3/19/2008	65	1364	119	16	5.2
KS08-11-MX1	3/19/2008	NA	214	131	81	2.4
KS08-108-MI1	8/1/2008	125	1321	116	26	8.0
KS08-108-MI2	8/1/2008	120	1344	ND	29	3.8
KS08-108-MX1	8/1/2008	NA	341	132	75	8.0
KS08-110-MI1	8/27/2008	150	922	88	59	3.8
KS08-110-MX1	8/27/2008	NA	318	116	82	1.0
KS08-112-MI1	9/2/2008	50	746	133	44	8.0
KS08-112-12-MI1	9/2/2008	50	1276	138	13	6.6
KS08-112-13-MI1	9/2/2008	90	1092	ND	4	5.2
KS08-112-16-MI1	9/2/2008	50	1135	ND	13	6.6
KS08-112-17-MI1	9/2/2008	45	863	ND	31	3.8
KS08-112-MX1	9/2/2008	NA	307	107	81	2.4
KS08-118-MI1	10/14/2008	90	723	141	63	6.6
KS08-118-MX1	10/14/2008	NA	396	70	76	3.8
KS09-152-MI1	9/17/2009	45	831	ND	51	8.0
KS09-152-MX1	9/17/2009	NA	519	ND	69	5.2
KS09-152H-2-MI1	9/17/2009	72	617	ND	62	5.2
KS09-152H-3-MI1	9/17/2009	64	1132	120	45	6.6
KS09-152H-4-MI1	9/17/2009	58	1113	ND	18	6.6
KS09-152H-5-MI1	9/17/2009	50	913	109	43	6.6
KS09-152H-6-MI1	9/17/2009	50	776	136	54	8.0
KS11-205-M1	1/17/2011	60	360	ND	74	2.4
KS11-205-MX1	1/17/2011	NA	436	85	78	3.8
KS13-262-MI1	6/4/2013	60	67	130	83	1.0
KS13-262-MX1	6/4/2013	NA	276	112	83	1.0
KS13-265-MI1	7/8/2013	30	603	ND	78	2.4
KS13-265-MI2	7/8/2013	35	376	180	80	5.2
KS13-265-MX1	7/8/2013	NA	256	118	84	1.0
KS13-266-MI1	8/9/2013	45	471	139	72	6.6
KS13-266-MI2	8/9/2013	25	67	91	68	9.4
KS13-266-MI3	8/9/2013	30	49	128	79	1.1
KS13-266-MI4	8/9/2013	35	283	105	75	6.6
KS13-266-MI5	8/9/2013	40	79	167	72	6.6
KS13-266-MI6	8/9/2013	45	61	162	80	1.0
KS13-266-MI7	8/9/2013	30	405	88	68	1.1
KS13-266-MI8	8/9/2013	30	135	71	84	2.4
KS13-266-MX1	8/9/2013	NA	459	150	84	1.0
KS14-271-MI1	1/10/2014	55	374	85	76	2.4
KS14-271-MI2	1/10/2014	30	116	172	74	2.4

KS14-271-MI3	1/10/2014	45	37	128	77	3.8
KS14-271-MI4	1/10/2014	47	442	ND	78	3.8
KS14-271-MI5	1/10/2014	50	538	117	86	3.8
KS14-271-MI6	1/10/2014	85	553	107	79	1.0
KS14-271-MI7	1/10/2014	25	49	183	77	2.4
KS14-271-MI8	1/10/2014	25	<30*	ND	73	8.0
KS14-276-MI1	3/18/2014	25	173	109	68	9.4
KS14-276-MI2	3/18/2014	45	532	116	75	2.4
KS14-276-MI3	3/18/2014	35	90	92	80	2.4
KS14-278-MI1	4/8/2014	35	<30*	84	78	5.2
KS14-278-MI2	4/8/2014	50	396	121	81	1.0
KS14-278-MI3	4/8/2014	50	463	113	73	8.0
KS14-278-MI4	4/8/2014	55	472	73	76	5.2
KS14-278-MI5	4/8/2014	50	<30*	155	81	1.0
KS14-278-MI6	4/8/2014	50	400	ND	79	9.4
KS14-278-MX1	4/8/2014	NA	190	114	81	1.0
KS14-279-MI1	4/22/2014	40	47	189	81	1.0
KS14-279-MI2	4/22/2014	35	347	199	81	1.0
KS14-279-MX1	4/22/2014	NA	304	102	82	2.4
KS15-314-MI2	4/28/2015	100	528	109	92	6.6
KS15-314-MX1	4/28/2015	NA	236	116	79	1.0
KS15-318-MI1	5/20/2015	63	172	ND	78	1.0
KE61-3142-MI1	?	120	319	ND	78	5.2
KE61-3142-MI2	?	90	346	ND	79	2.4
KS16-377-MI1	8/8/2016	50	391	ND	76	5.2
KS16-377-MI2	8/8/2016	50	301	ND	72	5.2
KS16-377-MX1	8/8/2016	NA	197	ND	73	6.6
KE62-3293S_1_G02-MI1	5/30/2018	110	925	85	62	6.6
KE62-3293S_1_G04-MI1	5/30/2018	100	1110	143	25	6.6
KE62-3293S_1_G04-MC2	5/30/2018	250	610	121	75	3.8
KE62-3293S_1_G04-MC3	5/30/2018	300	730	144	69	5.2
KE62-3293S_1_G05-MI1	5/30/2018	90	850	113	59	8.0
KE62-3293S_1_G06-MI1	5/30/2018	80	750	146	61	6.6
KE62-3293S_1_G06-MI2	5/30/2018	70	750	124	62	6.6
KE62-3293S_1_G06-MI3	5/30/2018	40	680	90	66	5.2
KE62-3293S_1_G06-MX1	5/30/2018	NA	350	157	79	2.4
KE62-3293S_1_G07-MX1	5/30/2018	NA	130	67	78	1.0

MI: melt inclusion, MX: matrix glass, ND: not determined, NA: not applicable, LCC: linear Cu complex.

^{*} S concentration below detection so set to the lower limit of detection (LLD) concentration of 30 ppm. a Sampling dates provided by HVO and generally are contemporaneous to the date of the eruptive event.

^b Relative measurement uncertainty estimated at 13% (1 σ).

^c Relative measurement uncertainty estimated at 15% (1σ).

^d Calculated % Cu¹⁺-oxide in glasses assuming binary mixing of Cu¹⁺-oxide and Cu¹⁺-sulfide species. Percentage based on linear component fitting (LCF) of spectral end-members.

^e Calculated residuals (*R-Factor*) between the fitted and measured spectra of the LCF. Better fits indicated by lower *R-Factors*.

Figure 1

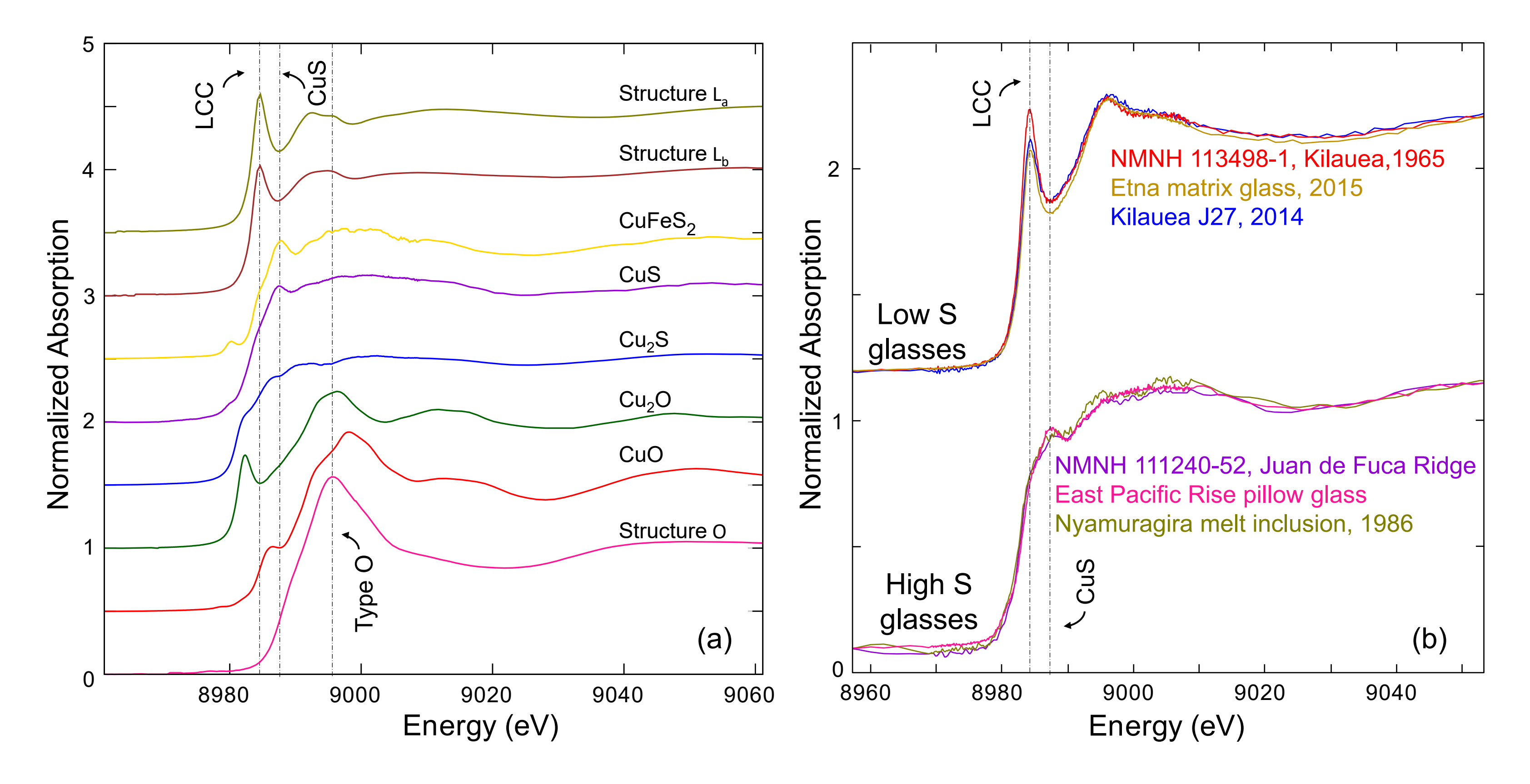


Figure 2 Figure 2

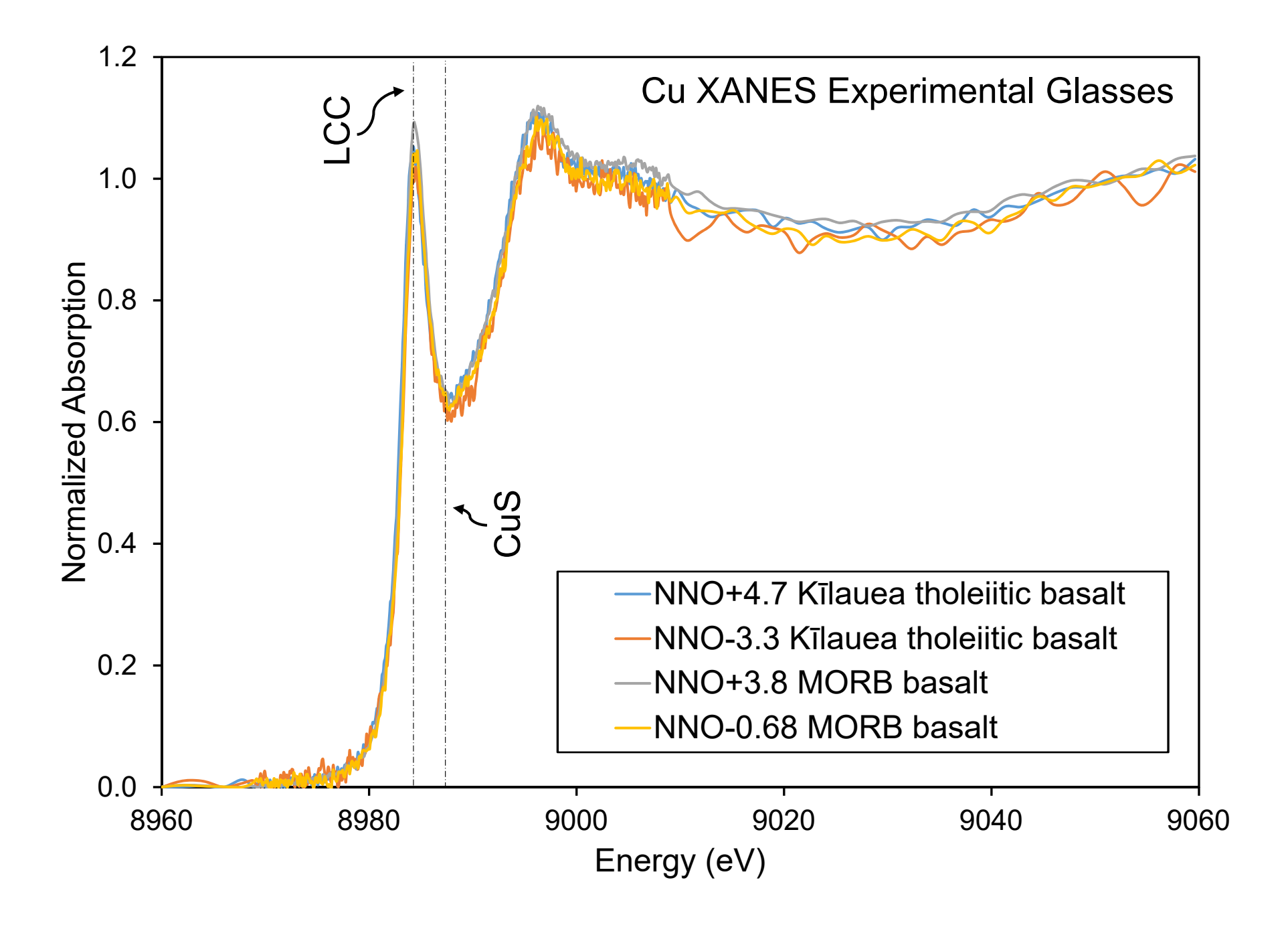


Figure 3 Figure 3

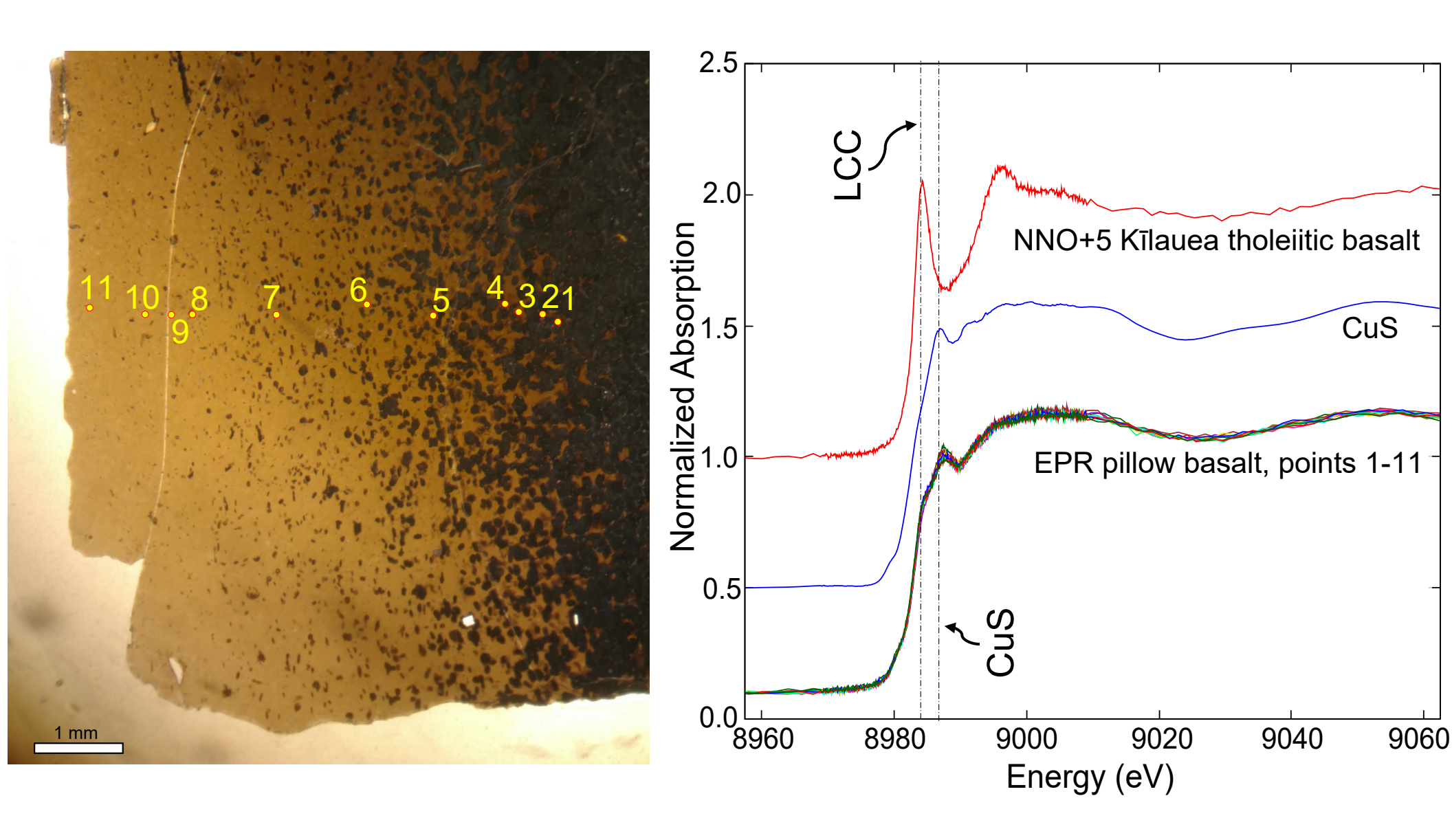
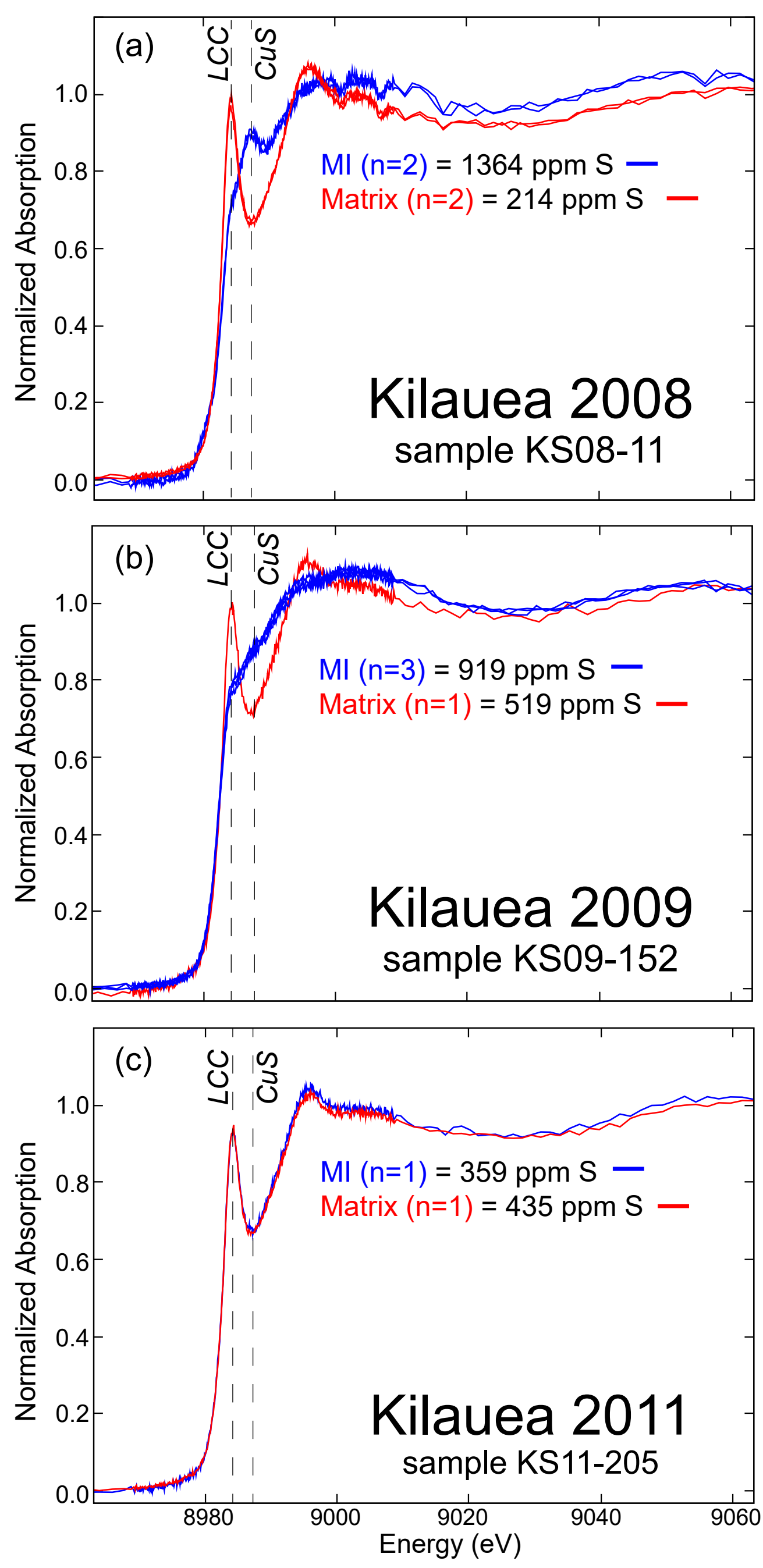


Figure 4



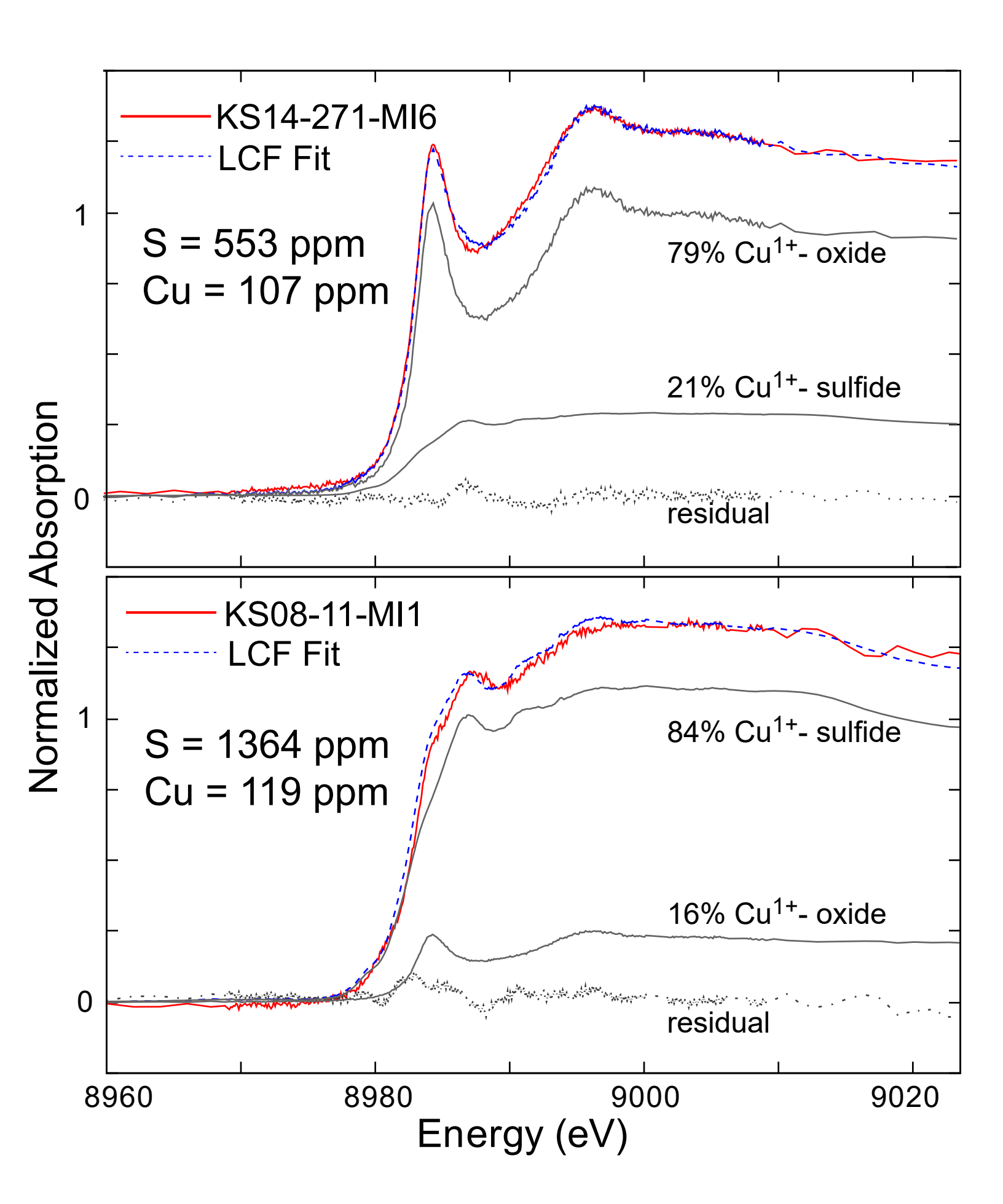


Figure 6 Figure 6

